Unified Electromagnetic Theory of Matter and Light

Section D — **Structure and Dynamics of the Universe**

Part D3 - **Magnetic Deflection of EM Waves**

Franc Rozman

Abstract

This paper develops a theoretical model of electromagnetic-wave deflection in nonuniform magnetic fields, based on the spatially structured electromagnetic-wave framework introduced in Parts B1–B4. Within this framework, a propagating electromagnetic wave is represented as a coherent tubular structure containing coupled electric E, magnetic B, and displacement-current-related P field configurations.

The proposed mechanism attributes magnetic deflection to the asymmetric interaction between the internal magnetic structure of the wave and an external magnetic-field gradient. The wave possesses inertia associated with its propagation energy, allowing a transverse magnetic force to change the direction of its momentum without introducing a nonzero rest mass. An effective force law is formulated in terms of the gradient of the external magnetic-field intensity, the wave's inertial energy, and its orientation relative to the magnetic field.

The resulting equations describe wave curvature and possible magnetic guidance. Three characteristic trajectories are obtained: gradual nonoscillatory alignment with a magnetic axis, faster alignment under critical damping, and damped transverse oscillations around the axis. The model also examines how internal E–B–P reorganization and directional electromagnetic radiation could contribute to transverse-momentum dissipation and changes in the wave's transverse dimensions.

Quantitative estimates and scaling relations identify conditions under which magnetic deflection may become approximately independent of the wave's transverse radius. Experimental tests are proposed to distinguish the predicted interaction from conventional optical and plasma effects.

The analysis establishes a mathematical framework for investigating magnetic deflection and guidance of structured electromagnetic waves. The microscopic origin of the effective magnetic coupling and the magnitude of radiative damping remain subjects for further theoretical and experimental investigation.

1. Introduction

The propagation of electromagnetic waves is conventionally described by Maxwell's equations, which establish the relationship between electric and magnetic fields, electromagnetic energy, and momentum. In vacuum, freely propagating electromagnetic waves follow straight trajectories unless they interact with matter, boundaries, or other physical influences.

The present study examines a proposed mechanism by which a spatially structured electromagnetic wave may change its propagation direction when passing through a nonuniform external magnetic field.

The investigation builds on the electromagnetic-wave model developed in Parts B1–B4. In this model, a propagating wave is represented as a coherent tubular electromagnetic structure containing coupled electric E, magnetic B, and intermediate displacement-current-related P field configurations. The fields continuously exchange energy and momentum while maintaining the propagation of the complete structure.

An essential feature of the proposed model is that the electromagnetic wave possesses inertia associated with its propagating energy. Consequently, a transverse force acting on the wave can change the direction of its momentum without requiring the introduction of a nonzero rest mass.

The central hypothesis investigated in this paper is that an external magnetic-field gradient can disturb the internal magnetic balance of the tubular wave. The resulting redistribution of electromagnetic stresses may produce a net transverse force and thereby change the propagation direction.

The magnitude and direction of this interaction are examined using an effective magnetic-force model that relates the transverse force to the spatial gradient of the external magnetic-field intensity. The possible dependence of the force on the angle between the propagation direction and the external magnetic field is also considered.

Particular attention is given to wave trajectories in magnetic-field configurations possessing a well-defined magnetic axis. Depending on the restoring magnetic force and the possible dissipation of transverse momentum, the model admits several types of behavior: gradual alignment with the magnetic axis, faster nonoscillatory alignment, and damped transverse oscillations around the axis.

The possible role of internal E–B–P reorganization and associated electromagnetic radiation is examined as a mechanism that may influence the stability and evolution of these trajectories.

The analysis distinguishes mathematical consequences of the proposed effective equations from physical assumptions that require further investigation. In particular, the interaction coefficient, angular dependence of the magnetic force, and magnitude of any radiative damping are not treated as independently established quantities.

The objective of this paper is to formulate a consistent mathematical framework connecting electromagnetic-wave inertia, magnetic interaction, transverse deflection, and possible magnetic guidance. The resulting equations provide a basis for quantitative estimates and for identifying experimental observations capable of testing the proposed mechanism.

The present study also provides the theoretical foundation for two subsequent investigations: Part D4, addressing the formation and optical characteristics of sunspots, and Part D5, examining the periodic luminosity variations of Cepheid stars. In both cases, the proposed

interaction between electromagnetic waves and nonuniform magnetic fields offers a possible mechanism for redirecting radiation and modifying its observed intensity. Conversely, the characteristic spatial structures of sunspots and the measured light curves of Cepheids provide observational constraints for evaluating the magnetic-deflection model developed in this paper. These applications therefore serve a dual purpose: they explore the explanatory potential of the proposed mechanism while offering independent opportunities to assess its physical validity and quantitative consistency.

2. Structure and Inertia of an Electromagnetic Wave

2.1. Tubular Structure of the Electromagnetic Wave

The electromagnetic-wave model developed in Parts B1–B4 represents a propagating wave as a continuous electromagnetic structure with a finite transverse extent.

The wave is described by its longitudinal wavelength λ, characteristic transverse radius R, electric-field amplitude E_0, and magnetic-field amplitude B_0.

The transverse structure is approximately rotationally symmetric around the direction of propagation. The electric and magnetic fields occupy related but not necessarily identical spatial distributions. Their interaction maintains the internal organization of the propagating electromagnetic wave.

The model distinguishes three coupled aspects of the internal field dynamics:

- The electric field E, associated with the positive energy contribution.
- The magnetic field B, associated in the proposed model with a negative internal binding-energy contribution.
- The intermediate configuration P, associated with displacement-current dynamics and the redistribution of electromagnetic energy and momentum.

The P configuration does not represent an independently established third Maxwell field. It describes a proposed intermediate stage in the internal evolution of the coupled electromagnetic structure.

In the absence of external disturbances, the transverse organization is assumed to remain approximately symmetric. The resulting propagation direction is defined by the total momentum of the wave.

The present investigation considers how this symmetry may be disturbed by an external magnetic field. [1]–[4]

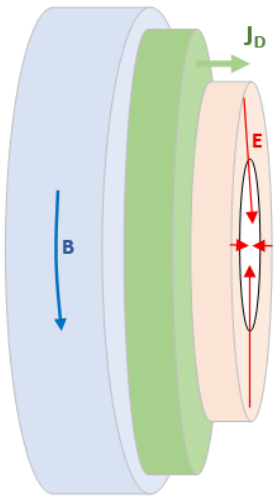


Figure 1. Internal structure of the proposed electromagnetic wave.
Schematic representation of the tubular electromagnetic structure, showing the spatial organization of the electric E and magnetic B fields and the displacement-current-related configuration P. The fields are coupled during propagation and

contribute to the internal energy and momentum dynamics of the wave. The illustration is conceptual and does not represent a complete quantitative field solution.

2.2. Internal Energy Balance

The model distinguishes between positive internal energy W_p and negative binding energy W_v:

$$W_p > 0, \qquad W_v < 0.$$

For a freely propagating electromagnetic wave, their magnitudes are assumed to be approximately balanced:

$$W_p + W_v \approx 0. \qquad (2.1)$$

This internal balance is not interpreted as the disappearance of electromagnetic energy or inertia.

The model separately identifies a positive propagation energy W_i, associated with the motion and momentum of the complete electromagnetic structure.

The intermediate P configuration participates in the redistribution of energy between the internal electromagnetic configurations. Its contribution must therefore be included consistently in the complete energy description, without counting the same energy more than once.

The detailed division of inertia among the internal configurations is not required for the trajectory analysis developed below. The relevant quantity is the total positive propagation energy of the selected coherent wave structure. [1]–[4]

2.3. Inertia and Momentum

A propagating electromagnetic wave carries energy and momentum even though its rest mass is zero.

The effective inertial mass associated with the propagation energy W_i is defined as

$$m_i = \frac{W_i}{c^2}. \qquad (2.2)$$

For a wave propagating at speed c, its momentum magnitude is

$$p = \frac{W_i}{c} = m_i c. \qquad (2.3)$$

The momentum vector is directed along the instantaneous propagation direction:

$$\mathbf{p} = \frac{W_i}{c}\hat{\mathbf{t}}. \qquad (2.4)$$

where $\hat{\mathbf{t}}$ is the unit tangent vector to the trajectory.

The effective inertial mass is not a rest mass. It expresses the resistance of the propagating electromagnetic energy to a change in its momentum.

When a transverse force acts on the wave, its momentum direction can change while its propagation speed remains approximately equal to c.

For approximately constant momentum magnitude, the transverse component of the force is

$$\mathbf{F}_\perp = \frac{W_i}{c}\frac{d\hat{\mathbf{t}}}{dt}. \qquad (2.5)$$

Since the wave propagates at speed c, the relation between time and path length s is

$$\frac{ds}{dt} = c.$$

Consequently,

$$\mathbf{F}_\perp = W_i \frac{d\hat{\mathbf{t}}}{ds}. \qquad (2.6)$$

This equation provides the mechanical basis for the magnetic-deflection analysis. [6], [7]

2.4. Energy and Transverse Dimensions

Parts B1–B2 introduce a hypothetical saturated electromagnetic-wave configuration characterized by approximately constant field amplitudes and geometrically similar transverse distributions.

For a coherent wave segment of length L, its propagation energy may be approximated by

$$W_i = C u_s R^2 L. \qquad (2.7)$$

where u_s is the characteristic saturated energy density and C is a dimensionless geometrical coefficient incorporating the spatial field distribution.

For constant u_s, C, and L, the transverse radius scales as

$$R \propto \sqrt{W_i}. \qquad (2.8)$$

Accordingly, a gradual reduction of propagation energy may be accompanied by a reduction of the transverse radius without necessarily destroying the coherent electromagnetic structure.

For small relative changes,

$$\frac{\Delta R}{R} \approx \frac{1}{2}\frac{\Delta W_i}{W_i}. \qquad (2.9)$$

This relationship is relevant when an electromagnetic wave loses energy while interacting with an external field.

The wavelength λ and transverse radius R represent different geometrical properties. The model does not require them to remain proportional.

The saturated energy density and characteristic field amplitudes have not yet been independently derived. Equation (2.7) therefore represents an approximate structural scaling relation rather than a complete numerical determination of wave inertia.

2.5. Transverse Momentum and Deflection

Consider an initially straight electromagnetic wave propagating along the z-axis.

Its initial momentum is

$$\mathbf{p}_0 = p\hat{\mathbf{z}}.$$

If an external interaction produces a transverse force F_x, the propagation direction changes.

For a small deflection angle θ,

$$p_x \approx p\theta.$$

Using $p = W_i/c$, the transverse equation of motion becomes

$$\frac{d\theta}{dt} = \frac{cF_x}{W_i}. \qquad (2.10)$$

provided that the momentum magnitude remains approximately constant.

For propagation predominantly along the z-axis,

$$\theta \approx \frac{dx}{dz}, \qquad dz \approx c\,dt.$$

Therefore,

$$\frac{d^2x}{dz^2} \approx \frac{F_x}{W_i}. \qquad (2.11)$$

This equation relates the curvature of an electromagnetic-wave trajectory directly to the transverse force and the propagation energy of the wave.

It is the starting point for the investigation of magnetic deflection.

The following section examines a proposed mechanism by which an external nonuniform magnetic field may disturb the

internal electromagnetic balance and produce the transverse force appearing in Equation (2.11). [1], [2], [4]

3. Interaction with an External Magnetic Field

3.1. Interaction of the Tubular Wave with an External Field

The preceding section represented a freely propagating electromagnetic wave as a coherent tubular structure with coupled E, B, and P configurations. In the unperturbed state, the transverse field organization is assumed to be approximately rotationally symmetric about the instantaneous propagation direction. This symmetry is relevant because a persistent transverse change in the momentum of the complete wave requires a corresponding net transverse interaction.

Consider an electromagnetic wave travelling through a prescribed, static external magnetic field $\mathbf{B}_e(\mathbf{r})$. The magnetic field associated with the wave itself is denoted by $\mathbf{B}_i(\mathbf{r}, t)$. Their total magnetic field is

$$\mathbf{B}_{\text{tot}} = \mathbf{B}_i + \mathbf{B}_e. \qquad (3.1)$$

The quantities $\mathbf{B}_i$ and $\mathbf{B}_e$ must be treated as vectors. Their squared magnitude is

$$B_{\text{tot}}^2 = B_i^2 + B_e^2 + 2\mathbf{B}_i \cdot \mathbf{B}_e. \qquad (3.2)$$

Thus, the interaction depends not only on the relative magnitudes of the two fields but also on their orientation and the spatial distribution of the internal wave field. In the proposed E–B–P description, an external magnetic field may modify this internal distribution and thereby affect the momentum balance of the whole propagating structure. The quantitative response of E and P to this disturbance is not yet specified by an independent dynamical law.

The interaction considered here is distinct from the standard propagation of light in classical vacuum electrodynamics: Maxwell's linear equations do not, by themselves, predict magnetic deflection of a freely propagating light wave by a prescribed static field in vacuum. The additional coupling examined below is therefore a testable hypothesis of the tubular-wave model. [6], [7]

3.2. Homogeneous External Magnetic Field

A homogeneous magnetic field has constant magnitude and direction over the wave's transverse extent:

$$\nabla B_e^2 = \mathbf{0}. \qquad (3.3)$$

A uniform external field can affect the local vector sum in Equation (3.1), and the internal tubular structure might reorganize in response. However, the effective gradient-dependent mechanism investigated in this study predicts no net transverse deflection when the field intensity is spatially uniform.

The resulting distinction is important: an internal change in field organization is not, by itself, equivalent to a change in the momentum direction of the entire wave. In particular, a local magnetic-pressure imbalance at a chosen section of the tube must be assessed together with the electric stresses, longitudinal surfaces, and complete momentum flux. Only a nonzero integrated transverse momentum transfer can bend its trajectory.

The homogeneous-field case therefore provides a useful reference condition for the model. A uniform field should not be assigned a net deflecting force merely

because the vector field distribution inside a chosen cross-section has changed. [6], [7]

3.3. Nonuniform Field and Transverse Magnetic Asymmetry

Now let the external magnetic field vary transversely across the wave. Let x denote the direction of the local transverse intensity gradient, and R the characteristic radius of the wave. If the external field varies on a much larger scale a_B, with $R \ll a_B$, its squared magnitude can be expanded near the wave axis at $x = x_c$:

$$B_e^2(x_c + \xi) \simeq B_e^2(x_c) + \xi \left.\frac{\partial B_e^2}{\partial x}\right|_{x_c}, \qquad |\xi| \lesssim R. \qquad (3.4)$$

Consequently, the two sides of the transverse structure encounter slightly different external magnetic intensities. On a circular section $\xi = R\cos\varphi$, the leading angular variation is proportional to $\cos\varphi$. This establishes the geometrical origin of the first-order asymmetry, without yet establishing the net force.

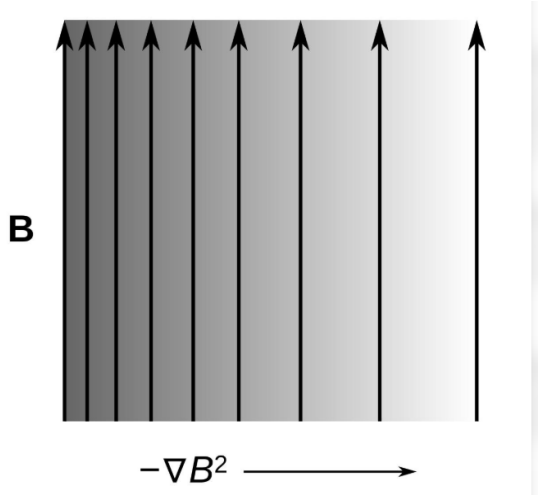


Figure 2. ***Spatial variation of an external magnetic field.*** *The parallel arrows represent the local magnetic-field direction, while the changing background intensity illustrates a transverse gradient of the magnetic-field magnitude. A tubular electromagnetic wave extending across this region encounters different external magnetic intensities on opposite sides of its transverse structure. This provides the geometric basis for the asymmetric magnetic interaction considered in the model.*

In the proposed model, the internal E–B–P configuration may respond by redistributing its magnetic field and momentum across the cross-section. For example, a perturbed magnetic magnitude can be written schematically as

$$B_i(r, \varphi) = B_0(r) + \varepsilon\, b_1(r)\cos\varphi + O(\varepsilon^2). \qquad (3.5)$$

Here ε is a dimensionless measure of asymmetry and $b_1(r)$ specifies its radial distribution. Equation (3.5) is a representation of field magnitude or of a selected field component, not a complete solution for the magnetic vector field. Any admissible three-dimensional field must satisfy $\nabla \cdot \mathbf{B}_{\mathrm{tot}} = 0$ and the corresponding Maxwell equations. Additional radial or longitudinal components may be required.

Because the internal magnetic field is coupled to E and the intermediate P configuration, a magnetic redistribution cannot in general be regarded as an isolated static deformation. Changes in internal energy flow and transverse momentum transport may accompany it. The direction and magnitude of the resulting net interaction are addressed by the effective description in Section 4. [6], [7]

3.4. Internal Magnetic Adjustment and the Boundary Region

One possible organizing hypothesis is that the tubular wave tends to maintain an approximately regulated total magnetic-field magnitude across its active region. In the special case where the internal and

external fields are locally orthogonal, this can be expressed as

$$B_i^2(r,\varphi) + B_e^2(r,\varphi) \simeq B_c^2, \qquad (3.6)$$

where B_c represents an assumed characteristic interior value. The corresponding internal magnitude would be

$$B_i \simeq \sqrt{B_c^2 - B_e^2}, \qquad B_e^2 \leq B_c^2. \qquad (3.7)$$

Thus, in this illustrative adjustment rule, the wave's internal magnetic magnitude is smaller on the side exposed to the stronger external field and larger on the opposite side. This is the compensation pattern suggested by the magnetic-step picture.

Equation (3.6) is a possible response condition, not a consequence of Maxwell's equations. If the fields are not orthogonal, the cross term in Equation (3.2) must be retained. Furthermore, nearly uniform magnetic energy density does not establish mechanical equilibrium: the magnetic stress depends on vector direction as well as field magnitude, and the electric and P-associated momentum transport must also be included.

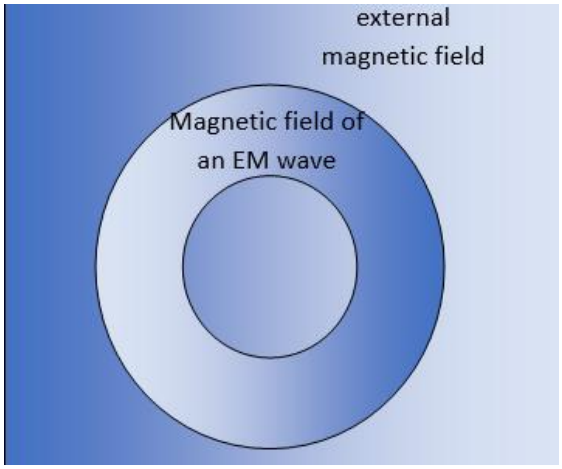


Figure 3. Internal magnetic-field adjustment in a nonuniform external magnetic field. *The diagram illustrates the proposed redistribution of the magnetic field within the tubular electromagnetic wave. The internal magnetic-field intensity decreases on the side exposed to the stronger external field and increases on the opposite side. This compensating response is assumed to maintain an approximately balanced total magnetic-field intensity across the wave structure. The resulting asymmetric boundary conditions provide a possible basis for the transverse magnetic interaction investigated in this study.*

At the boundary of the active tubular region, the internal field decreases toward the surrounding external field. A simplified diagram may therefore show a change in magnetic intensity across a narrow transition zone, sometimes described here as a *magnetic step*. A physical electromagnetic boundary, however, must have a field profile consistent with the field equations; the schematic step should not be interpreted as an unrestricted discontinuity or as an automatically established force.

In standard electrodynamics, the magnetic part of the Maxwell stress tensor is

$$\mathbf{T}_B = \frac{1}{\mu_0}\left(\mathbf{BB} - \frac{1}{2}B^2\mathbf{I}\right). \qquad (3.8)$$

This tensor contains both transverse pressure-like and directional tension-like contributions. The total electromagnetic momentum balance also involves electric stresses and field momentum. The proposed negative magnetic *binding-energy* convention used for the internal E–B–P organization does not, by itself, reverse the sign of the Maxwell stress or prove attraction toward stronger external fields.

The boundary interpretation consequently motivates a candidate coupling mechanism, but its magnitude and sign

remain to be established by the complete field interaction or by experiment. [6], [7]

3.5. Orientation of the Wave and the External Field

Let $\hat{\mathbf{t}}$ denote the instantaneous direction of wave propagation and $\hat{\mathbf{b}} = \mathbf{B}_e/B_e$ the local direction of the external magnetic field. Their relative angle α is defined by

$$\cos\alpha = \hat{\mathbf{t}} \cdot \hat{\mathbf{b}}. \qquad (3.9)$$

The working hypothesis explored in this paper is that the effective transverse interaction becomes weaker as the propagation direction departs from alignment with the magnetic field. A simple orientation factor satisfying this requirement and remaining unchanged under reversal of field direction is

$$g(\alpha) = \cos^2\alpha. \qquad (3.10)$$

According to this trial law, the coupling is greatest for parallel or antiparallel propagation and vanishes at $90°$. This factor must not be confused with the geometrical projection of a force onto the direction perpendicular to the trajectory. Even when $g(\alpha)$ is maximal, the net transverse force is zero if the transverse gradient itself vanishes.

The form of Equation (3.10) has not been derived from a complete E–B–P dynamics and should therefore be regarded as a assumption. Other angular responses are possible; their consequences can be compared against observations without altering the inertial framework of Section 2.

3.6. From Internal Asymmetry to a Net Transverse Interaction

The purpose of this section has been to identify the structural circumstances under which the proposed tubular wave could experience a magnetic deflection. They can be summarized as follows. A homogeneous external field does not produce a net force in the adopted gradient mechanism. A nonuniform field introduces a leading transverse asymmetry of the external magnetic intensity. The wave may respond through a coupled adjustment of its internal magnetic, electric, and P-associated momentum distributions. Such an adjustment may create an effective transverse interaction, but the boundary picture alone does not establish its sign or coefficient.

For the next stage it is useful to distinguish the gradient perpendicular to the instantaneous propagation direction:

$$\nabla_\perp B_e^2 = (\mathbf{I} - \hat{\mathbf{t}}\hat{\mathbf{t}}^\mathsf{T})\nabla B_e^2. \qquad (3.11)$$

This quantity identifies the variation in external magnetic intensity capable of changing the direction of propagation, as distinct from a longitudinal variation that may affect energy or other aspects of the interaction.

Section 4 introduces an explicit effective transverse-force law involving $\nabla_\perp B_e^2$, the angle factor $g(\alpha)$, and a dimensionless interaction coefficient χ. That law will be analyzed as a physical hypothesis rather than inferred solely from the schematic magnetic step. The resulting force is then combined with the inertia and momentum relations of Section 2 to obtain the curvature of the wave trajectory.

4. Magnetic Force and Deflection

4.1. Momentum Balance of the Propagating Wave

Section 2 introduced the positive propagation energy W_i of a selected

coherent wave segment and its momentum $\mathbf{p} = (W_i/c)\hat{\mathbf{t}}$, where $\hat{\mathbf{t}}$ is the local propagation direction. Section 3 identified a transverse intensity gradient of the external magnetic field as a possible source of asymmetry in the wave's internal E–B–P organization. We now formulate the resulting deflection as an effective, testable force law.

For a wave segment subject to a net external force $\mathbf{F}$, the momentum balance is

$$\frac{d\mathbf{p}}{dt} = \mathbf{F}. \qquad (4.1)$$

Writing $\mathbf{p} = p\hat{\mathbf{t}}$ separates changes in momentum magnitude from changes in its direction:

$$\frac{d\mathbf{p}}{dt} = \frac{dp}{dt}\hat{\mathbf{t}} + p\frac{d\hat{\mathbf{t}}}{dt}. \qquad (4.2)$$

Only the second term bends the path. With $p = W_i/c$ and $ds/dt = c$, the component perpendicular to the instantaneous direction is

$$\boxed{\mathbf{F}_\perp = W_i\frac{d\hat{\mathbf{t}}}{ds}}. \qquad (4.3)$$

Equation (4.3) remains the local directional balance when the energy changes slowly, provided the relation $p = W_i/c$ continues to hold and the force includes all transverse momentum transferred to or from the selected segment. Changes in longitudinal momentum and energy require a separate balance. This distinction becomes important in the discussion of radiation losses in Section 5. [5]–[7]

4.2. Effective Magnetic-Force Hypothesis

Let $\mathbf{B}_e(\mathbf{r})$ be the external magnetic field. Define the transverse gradient of its squared magnitude as

$$\nabla_\perp B_e^2 = (\mathbf{I} - \hat{\mathbf{t}}\hat{\mathbf{t}}^{\mathsf{T}})\nabla B_e^2. \qquad (4.4)$$

We investigate the constitutive hypothesis

$$\boxed{\mathbf{F}_\perp^{\mathrm{mag}} = \frac{\chi V_{\mathrm{eff}}}{2\mu_0}\, g(\alpha)\, \nabla_\perp B_e^2}. \qquad (4.5)$$

Here V_{eff} is the effective interaction volume of the same coherent wave segment whose energy is W_i; χ is a dimensionless magnetic-response coefficient; and $g(\alpha)$ accounts for the angle between propagation and the external magnetic-field direction. As proposed in Section 3, one simple trial relation is

$$\cos\alpha = \hat{\mathbf{t}}\cdot\hat{\mathbf{b}}, \qquad g(\alpha) = \cos^2\alpha, \qquad \hat{\mathbf{b}} = \frac{\mathbf{B}_e}{B_e}. \qquad (4.6)$$

The formula is applied where $B_e \neq 0$. With $\chi > 0$, it describes deflection toward greater B_e^2; reversing the direction of the external field does not reverse the force. With $\chi = 0$, no additional magnetic deflection is predicted. The idealized choice $\chi = 1$ is a reference hypothesis, not a value derived from Maxwell's equations or from the schematic magnetic boundary.

The effective factor $g(\alpha)$ must not be confused with the transverse projection in Equation (4.4). The former is a proposed physical dependence of the coupling; the latter is a geometrical necessity when computing curvature. In particular, a strong field or a favorable orientation cannot bend a path if the *transverse* intensity gradient is zero.

Equation (4.5) is an additional hypothesis of the structured-wave description. The linear vacuum Maxwell equations do not predict deflection of a freely propagating electromagnetic wave solely by a static external magnetic field. Any nonzero χ must therefore be supported by a consistent additional interaction mechanism or by experimental evidence. [5]–[7]

4.3. Magnetic Boundary, Energy, and the Sign of the Force

The "magnetic step" introduced in Section 3 illustrates how different external magnetic intensities may appear on opposite sides of the wave's transverse structure. However, the direction of the net force cannot be read directly from a scalar pressure difference or from the negative sign assigned to the model's internal magnetic binding energy.

For example, consider a hypothetical isotropic pressure jump $\Delta p = (B_c^2 - B_e^2)/(2\mu_0)$ on a circular transverse boundary. Integrating its normal force in a slowly varying transverse field gives

$$f_x^{\text{scalar}} = -\frac{A}{2\mu_0}\frac{dB_e^2}{dx}, \qquad (4.7)$$

where A is the enclosed effective cross-sectional area and f_x is force per unit longitudinal length. This simplified pressure construction points toward *weaker*, rather than stronger, magnetic intensity. It is not a complete electromagnetic stress calculation: the full Maxwell tensor includes directional magnetic tension, electric stress, and longitudinal momentum flow.

An attractive force of the form (4.5) can be represented phenomenologically, for a fixed orientation factor and fixed volume, by a local interaction-energy function

$$U_{\text{int}} = -\chi\frac{V_{\text{eff}}}{2\mu_0}\, g(\alpha) B_e^2. \qquad (4.8)$$

The *position* derivative of this energy reproduces the gradient part of Equation (4.5) if χ, V_{eff}, and g are held fixed. When g depends on the trajectory direction, Equation (4.8) does not by itself provide a complete conservative dynamical derivation; directional derivatives and possible longitudinal energy exchange require independent treatment. Thus the energy expression is an interpretation of the adopted force law, not a proof of it.

The coefficient χ can ultimately be evaluated only through the actual coupled field response and momentum flux, or constrained experimentally. For the present analysis it remains explicit. [5]–[7]

4.4. Curvature of the Wave Trajectory

Combining Equations (4.3) and (4.5) yields the vector curvature equation

$$\boxed{\frac{d\hat{\mathbf{t}}}{ds} = \frac{\chi V_{\text{eff}}}{2\mu_0 W_i}\, g(\alpha)\, \nabla_\perp B_e^2.} \qquad (4.9)$$

The curvature magnitude $\kappa = 1/\rho$ (ρ being the local radius of curvature) is therefore

$$\boxed{\kappa = \frac{\chi V_{\text{eff}}}{2\mu_0 W_i}\, g(\alpha)\, |\nabla_\perp B_e^2|.} \qquad (4.10)$$

This relation states that a greater transverse magnetic-intensity gradient produces greater curvature, whereas greater propagation energy produces greater resistance to deflection for the same effective interaction volume. The dependence on V_{eff}/W_i is essential: one must not compare the force on an entire coherent segment with the energy of only a small part of it.

For a mainly longitudinal trajectory $\mathbf{r}(z) = (x(z), 0, z)$ with $|dx/dz| \ll 1$, the local approximation becomes

$$\boxed{\frac{d^2x}{dz^2} \simeq \frac{\chi V_{\text{eff}}}{2\mu_0 W_i}\, g(\alpha)\, \frac{\partial B_e^2}{\partial x}.} \qquad (4.11)$$

The derivative in (4.11) is evaluated along the wave path, and the reduction assumes that the neglected corrections from the transverse projection are small. For larger angles, Equation (4.9), rather than the paraxial form, should be integrated.

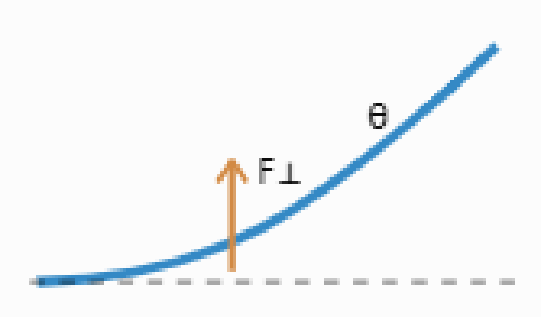


Figure 4. Deflection of an electromagnetic-wave trajectory under a transverse force. The blue curve represents the propagation path, while the arrow indicates the transverse force responsible for changing the direction of the wave momentum. The angle θ describes the resulting deviation from the initial propagation direction. The curvature depends on the ratio between the transverse force and the wave's propagation energy, as expressed by the effective model.

4.5. Dependence on Transverse Wave Dimensions

For the approximately saturated structures considered in Section 2, write the propagation energy and interaction volume as

$$W_i = C\,u_s R^2 L, \qquad V_{\text{eff}} = C_V R^2 L. \qquad (4.12)$$

Here C and C_V specify the energy and interaction profiles, respectively. Substitution into Equation (4.10) gives

$$\boxed{\kappa = \frac{\chi C_V}{2\mu_0 C u_s}\, g(\alpha)\,|\nabla_\perp B_e^2|.} \qquad (4.13)$$

Within this restricted family of geometrically similar saturated waves, the explicit factors $R^2 L$ cancel. The effective model thus allows equal curvature for different transverse radii when u_s, χ, C_V/C, and the external-field geometry are the same. It does *not* establish universal wavelength independence: the internal field profiles or the response coefficient may depend on wavelength, coherence, or other wave properties.

A decrease of wave energy accompanied by $R \propto \sqrt{W_i}$ need not, by itself, change the curvature if the above similarity assumptions remain valid. A change of internal saturation, coherence, or geometry can break this cancellation.

4.6. Local Example: A Gaussian Magnetic-Intensity Profile

To make the directional effect explicit, consider a magnetic-intensity maximum centered on the z axis,

$$B_e^2(x) = B_m^2 \exp(-x^2/a^2), \qquad (4.14)$$

where a is a characteristic transverse scale. This equation specifies a scalar intensity profile; it is not, by itself, a complete vector magnetic-field solution. The local field direction and its consistency with $\nabla \cdot \mathbf{B}_e = 0$ must be specified for a physical configuration and for evaluating α.

Differentiation gives

$$\frac{dB_e^2}{dx} = -\frac{2B_m^2 x}{a^2}\exp(-x^2/a^2). \qquad (4.15)$$

For a nearly axial wave with $g(\alpha) \simeq 1$, Equation (4.11) takes the form

$$\boxed{\frac{d^2x}{dz^2} = -\frac{\chi V_{\text{eff}} B_m^2}{\mu_0 W_i a^2}\, x\exp(-x^2/a^2).} \qquad (4.16)$$

For $\chi > 0$, the transverse acceleration is directed toward the intensity maximum. Close to the axis, $|x| \ll a$, it is approximately linear in x. The character of the resulting trajectories and the possible effect of radiative damping are treated in Section 5.

The example also shows an essential limitation: if the magnetically nonuniform region has finite longitudinal extent, an incoming wave may leave it before reaching the axis. A restoring force alone therefore does not guarantee permanent magnetic capture.

4.7. Scope and Testable Consequences

The present section establishes a mathematical relationship between the transverse force acting on a propagating electromagnetic wave and the resulting curvature of its trajectory. Given the effective magnetic-force hypothesis expressed by Equation (4.5), the curvature relations (4.9)–(4.11) follow directly from the momentum balance of the wave.

The proposed model predicts no gradient-induced deflection in a homogeneous magnetic field. In a nonuniform field, the deflection depends on the transverse gradient of the squared magnetic-field magnitude, the propagation energy of the wave, and its orientation relative to the external field. For geometrically similar saturated electromagnetic structures, the explicit dependence on transverse radius may cancel.

The central physical hypothesis is that the asymmetric magnetic interaction produces a net force directed toward stronger magnetic-field intensity. The proposed internal magnetic adjustment and the magnetic-step interpretation provide a possible structural explanation, but they do not independently establish the direction or magnitude of this force. Consequently, the interaction coefficient (\chi), including its sign and possible dependence on wave structure, remains to be determined. The assumed angular dependence $g(\alpha) = (\cos\alpha)^2$ likewise requires independent verification.

These uncertainties do not prevent quantitative examination of the model. Measurements of deflection as a function of magnetic-field strength, transverse gradient, and propagation angle can constrain the effective coupling relative to the wave's inertial energy density. In particular, the predicted dependence on the squared magnetic-field magnitude and the proposed angular response provide experimentally distinguishable consequences. A sufficiently sensitive null result would place an upper limit on the effective coupling and could exclude specific parameter choices.

Section 5 extends this framework to trajectories in nonuniform magnetic fields. It distinguishes deflection without dissipation from gradual alignment with a magnetic axis, which would additionally require a mechanism for removing transverse momentum, potentially through directional radiation associated with internal E–B–P reorganization.

5. Trajectories in Nonuniform Magnetic Fields

5.1. From Magnetic Force to the Trajectory Equation

Section 4 established an effective transverse-force hypothesis for a coherent electromagnetic-wave segment. In this section, the same hypothesis is used to calculate trajectories, first without dissipation and then with a possible radiative loss of transverse momentum. The distinction is important: a force

directed toward a magnetic axis does not, by itself, require the wave to remain on that axis.

Let $\mathbf{r}(s)$ denote the trajectory parameterized by path length s, and let $\hat{\mathbf{t}} = d\mathbf{r}/ds$ be its unit tangent. With the propagation energy W_i and the momentum relation $\mathbf{p} = (W_i/c)\hat{\mathbf{t}}$, the transverse momentum balance is

$$\boxed{\frac{d\hat{\mathbf{t}}}{ds} = \frac{\chi V_{\text{eff}}}{2\mu_0 W_i}\, g(\alpha)(\mathbf{I} - \hat{\mathbf{t}}\hat{\mathbf{t}}^{\top})\nabla B_e^2.} \qquad (5.1)$$

This equation describes the change of direction induced by the proposed effective magnetic force. The coefficient χ is not independently determined; the trial angular factor is $g(\alpha) = \cos^2\alpha$, with α the angle between $\hat{\mathbf{t}}$ and the local external field. The vector projection ensures that only the force perpendicular to the path contributes to curvature.

For motion predominantly along the z direction and a small slope $|x'(z)| \ll 1$, where a prime denotes d/dz, Equation (5.1) becomes

$$\boxed{x''(z) \simeq \frac{\chi V_{\text{eff}}}{2\mu_0 W_i}\, g(\alpha)\, \partial_x B_e^2(x, z).} \qquad (5.2)$$

The ratio V_{eff}/W_i must be evaluated for the same coherent wave segment. In deriving (5.2), the longitudinal variation of energy and the higher-order corrections associated with the changing tangent have been neglected. The full vector form (5.1) should be used when deflection angles are not small.

5.2. Guiding Field and Restoring Force Near Its Axis

Consider an extended magnetic structure whose field intensity is greatest on its central axis, $x = 0$. A convenient illustrative transverse profile is

$$B_e^2(x) = B_m^2 \exp(-x^2/a^2), \qquad (5.3)$$

where B_m is the axial field magnitude and a is the characteristic transverse width. For an approximately axial field direction, a corresponding static divergence-free idealization is $\mathbf{B}_e = B_m \exp[-x^2/(2a^2)]\,\hat{\mathbf{z}}$, independent of z. A finite-length magnetic configuration requires additional field components satisfying $\nabla \cdot \mathbf{B}_e = 0$.

Differentiation gives

$$\partial_x B_e^2 = -\frac{2xB_m^2}{a^2} \exp(-x^2/a^2). \qquad (5.4)$$

For $\chi > 0$, the assumed transverse force is directed toward the axis on either side. For nearly axial propagation, $g(\alpha) \simeq 1$, and Equation (5.2) becomes

$$\boxed{x'' = -\frac{2\eta}{a^2}\, x \exp(-x^2/a^2), \quad \eta = \frac{\chi V_{\text{eff}} B_m^2}{2\mu_0 W_i}.} \qquad (5.5)$$

The dimensionless parameter η measures the effective magnetic interaction relative to the propagation energy. Close to the axis, where $|x| \ll a$, the equation is approximately linear:

$$\boxed{x'' + k_g^2 x = 0, \qquad k_g^2 = \frac{2\eta}{a^2} = \frac{\chi V_{\text{eff}} B_m^2}{\mu_0 W_i a^2}.} \qquad (5.6)$$

The parameter k_g has dimensions of inverse length. It is a *spatial* oscillation constant, not the angular frequency of the electromagnetic carrier wave. This distinction avoids confusing transverse trajectory variations with the much faster internal E–B–P evolution.

5.3. Deflection Without Damping

For a wave entering the near-axis region at $z = 0$, with initial transverse displacement x_0 and slope θ_0, the undamped solution of Equation (5.6) is

$$\boxed{x(z) = x_0\cos(k_g z) + \frac{\theta_0}{k_g}\sin(k_g z).} \quad (5.7)$$

A wave initially parallel to the axis ($\theta_0 = 0$) moves toward it and reaches it for the first time at

$$\boxed{z_{\text{axis}} = \frac{\pi}{2k_g}.} \quad (5.8)$$

It normally crosses the axis because its transverse momentum does not vanish there. In a sufficiently long idealized guiding field, the resulting path oscillates about the axis. The central axis is therefore a restoring equilibrium trajectory, but not an automatic absorbing or capturing boundary.

The same conclusion can be expressed through a conserved paraxial quantity:

$$\mathcal{H}_\perp = \frac{1}{2}(x')^2 + \frac{1}{2}k_g^2 x^2, \qquad \frac{d\mathcal{H}_\perp}{dz} = 0. \quad (5.9)$$

The quantity $\mathcal{H}_\perp$ is a normalized trajectory integral, not the total electromagnetic energy. Its constancy shows why transverse oscillations cannot decay without another interaction. A realistic magnetic region may terminate before the first axis crossing; the outgoing wave then continues along the direction attained at the exit.

5.4. Finite Magnetic Regions and Net Angular Deflection

The magnetic intensity may vary along the propagation direction as well as transversely. For a localized illustrative profile, take

$$B_e^2(x,z) = B_m^2 \exp\left(-\frac{x^2}{a^2} - \frac{z^2}{\ell^2}\right), \quad (5.10)$$

where ℓ denotes the longitudinal extent of the interaction. Equation (5.10) specifies a scalar intensity profile; its full vector realization must satisfy the magnetic divergence constraint and is not uniquely specified by this formula.

For small deflections, the transverse coordinate may be approximated by the impact parameter b while integrating the change in slope. With $g(\alpha) \simeq 1$ and a nearly constant ratio V_{eff}/W_i, Equation (5.2) gives

$$\boxed{\theta_{\text{out}} \simeq -\frac{2\sqrt{\pi}\,\eta\ell b}{a^2}\exp(-b^2/a^2).} \quad (5.11)$$

The negative sign indicates deflection toward the axis for an incident wave with $b > 0$. The magnitude is maximal at $|b| = a/\sqrt{2}$ within this first-order approximation. A localized magnetic profile can thus change the outgoing direction without permanently guiding the wave.

As an illustration, let $a = 1000\ \text{km}$, $\ell = 2000\ \text{km}$, $b = 500\ \text{km}$, and $\eta = 10^{-5}$. Equation (5.11) gives $\theta_{\text{out}} \simeq -2.76 \times 10^{-5}$ rad, or about -5.69 arcseconds. The numerical value of η is chosen for illustration, not derived from the internal electromagnetic structure. The result is therefore a conditional trajectory calculation, not a parameter-free prediction.

5.5. Radiation, Momentum Loss, and Effective Damping

The internal E–B–P configuration may be disturbed during magnetic deflection. One possible consequence is additional

radiation. However, energy loss and damping of transverse motion must be distinguished: radiation emitted symmetrically around the instantaneous propagation direction reduces the wave energy but does not, by itself, decrease its angle with respect to the magnetic axis.

Let P_{rad} be the radiated power and Q_x the rate at which the radiation carries transverse momentum away. Neglecting other energy exchanges for this local balance,

$$\frac{dW_i}{dt} = -P_{\mathrm{rad}}, \qquad \frac{dp_x}{dt} = F_{\mathrm{mag},x} - Q_x. \qquad (5.12)$$

With $p_x \simeq (W_i/c)\theta$, differentiation yields

$$\boxed{\frac{d\theta}{dt} = \frac{cF_{\mathrm{mag},x}}{W_i} - \frac{cQ_x - P_{\mathrm{rad}}\theta}{W_i}.} \qquad (5.13)$$

If radiation carries momentum along the wave direction, $Q_x = (P_{\mathrm{rad}}/c)\theta$, the radiative contribution to the angular change vanishes. For damping, an excess outward transverse momentum flux is necessary. A simple local phenomenological closure is

$$\frac{cQ_x}{P_{\mathrm{rad}}} = (1+\zeta)\theta, \qquad \zeta > 0, \qquad (5.14)$$

where ζ characterizes the directional asymmetry of the radiated momentum relative to the moving wave. Such a relation is meaningful only for sufficiently small slopes and a physically realizable emission pattern. The corresponding trajectory equation is

$$\boxed{x'' + \gamma x' + k_g^2 x = 0, \quad \gamma = \frac{\zeta P_{\mathrm{rad}}}{cW_i}.} \qquad (5.15)$$

The coefficient γ has dimensions of inverse length. Equation (5.15) is a local effective description that assumes slowly changing γ and k_g. A time-dependent deformation of P does not by itself prove that $\zeta > 0$: this sign must follow from a calculation of the angular distribution of the actual outgoing radiation.

Indeed, the transverse radiation-momentum flux can be defined as

$$Q_x = \frac{1}{c}\int n_x \frac{dP_{\mathrm{rad}}}{d\Omega}\, d\Omega. \qquad (5.16)$$

A symmetric emission pattern can yield $Q_x = 0$ in the laboratory frame or yield the component expected along the wave direction without any damping. Only an appropriate directional asymmetry produces the extra term required by Equation (5.14). [5], [6]

5.6. Three Possible Guided Trajectories

Equation (5.15) admits three characteristic regimes, according to the ratio between the damping constant and the restoring spatial constant. They are alternative mathematical outcomes of the *same* effective model, not three separate force laws.

Slow nonoscillatory approach (overdamping). When $\gamma > 2k_g$, the characteristic roots are real and negative:

$$r_{\pm} = \frac{-\gamma \pm \sqrt{\gamma^2 - 4k_g^2}}{2}. \qquad (5.17)$$

For a wave initially parallel to the axis, $x(0) = x_0$ and $x'(0) = 0$, the displacement is a sum of decaying exponentials. It approaches the axis without crossing it; sufficiently strong damping produces a slow final approach.

Fast nonoscillatory approach (critical damping). When $\gamma = 2k_g$, the solution for the same initial conditions becomes

$$\boxed{x(z) = x_0(1 + k_g z)e^{-k_g z}.} \qquad (5.18)$$

This is the critical-damping limit and provides the fastest nonoscillatory return for the specified linear model and initial conditions.

Damped oscillations about the axis (underdamping). When $0 < \gamma < 2k_g$, define

$$q = \sqrt{k_g^2 - \gamma^2/4}. \qquad (5.19)$$

For $x(0) = x_0$ and $x'(0) = 0$, the displacement is

$$\boxed{x(z) = x_0 e^{-\gamma z/2}\left[\cos(qz) + \frac{\gamma}{2q}\sin(qz)\right].} \qquad (5.20)$$

The wave may cross the magnetic axis several times, but its oscillation envelope decreases approximately as $e^{-\gamma z/2}$. This permits gentle oscillatory guidance rather than requiring immediate alignment exactly on the axis. For $\gamma = 0$, the oscillation does not decay.

These results assume that a guiding field persists over a sufficiently long distance. If the wave leaves the nonuniform magnetic region, its subsequent path is determined by the momentum it retains at the exit. For arbitrary incident angle or strong spatial gradients, the nonlinear, angle-dependent equations must be integrated instead of using the local linear solutions.

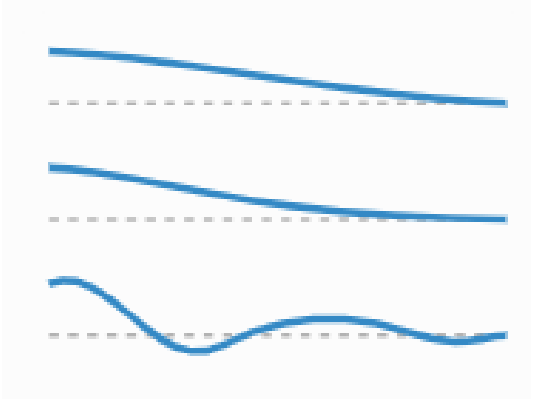


Figure 5. ***Three possible trajectories of an electromagnetic wave in a magnetic guiding field.*** *The dashed lines represent the magnetic axis, while the solid curves illustrate gradual nonoscillatory alignment, faster nonoscillatory alignment, and damped transverse oscillations around the axis. These trajectories correspond to different damping regimes of the effective wave-guidance equation. Their occurrence depends on the restoring magnetic interaction, the directional momentum loss, and the longitudinal extent of the guiding field.*

5.7. Coupling Between Damping and Transverse Radius

A radiative loss of propagation energy may also modify the transverse geometry of the coherent electromagnetic structure. Under the saturated, fixed-length scaling assumption introduced in Section 2,

$$W_i = Cu_s R^2 L, \qquad \frac{R(z)}{R_0} = \sqrt{\frac{W_i(z)}{W_{i0}}}. \qquad (5.21)$$

If the relative energy loss per unit propagation distance is approximately constant, $dW_i/dz = -W_i/L_E$, then

$$\boxed{W_i(z) = W_{i0}e^{-z/L_E}, \qquad R(z) = R_0 e^{-z/(2L_E)}.} \qquad (5.22)$$

Under the directional-radiation closure (5.14), $\gamma = \zeta/L_E$. Therefore transverse alignment and radius reduction can be related within a particular emission model, but one does not imply the other. In particular, a shrinking radius alone is not evidence for damping of the propagation angle. If the internal geometry, the

coherent length, or the response coefficient varies significantly, both the simple radius law and the constant-coefficient trajectory equation must be reconsidered. [5], [6]

5.8. Physical Interpretation and Limits

The effective trajectory model separates three mechanisms. First, the assumed magnetic-gradient force changes the direction of the wave momentum. Second, the finite extent and geometry of the external field determine whether the wave merely acquires a deflection angle or remains within a guiding region. Third, directional radiation could remove transverse momentum and allow a gradual approach to the magnetic axis.

The three guided trajectories described above—slow approach, critical nonoscillatory approach, and damped oscillation—are mathematically consistent solutions of Equation (5.15). Their occurrence in nature is not yet established. The attractive sign and magnitude of the coefficient χ, the angular factor $g(\alpha)$, and the damping coefficient γ require an independent electromagnetic momentum-flux calculation or experimental constraints. The static magnetic field itself does not provide this extra interaction in ordinary linear vacuum electrodynamics.

The next section develops quantitative scaling relations and representative numerical estimates. Its purpose is to identify which combinations of field strength, gradient scale, energy density, and response coefficients would make the proposed deflection measurable.

6. Quantitative Estimates and Scaling Laws

6.1. Purpose and Controlling Parameters

Sections 4 and 5 established an effective magnetic-deflection model based on the transverse momentum of a coherent electromagnetic-wave segment. The present section examines the magnitude and scaling of the resulting trajectory changes. The objective is not to assign an experimentally established value to the magnetic-response coefficient, but to identify which combinations of wave properties and external field parameters control the predicted deflection.

For a nearly straight wave with propagation energy W_i, effective interaction volume V_{eff}, and trial angular factor $g(\alpha)$, the paraxial equation is

$$\boxed{x''(z) \simeq \frac{\chi V_{\mathrm{eff}}}{2\mu_0 W_i}\, g(\alpha)\, \frac{\partial B_e^2(x,z)}{\partial x}.} \qquad (6.1)$$

The response coefficient χ is dimensionless; μ_0 is the vacuum permeability, B_e the magnitude of the external magnetic field, and α the angle between the local field and the propagation direction. The adopted trial function is $g(\alpha) = \cos^2\alpha$. The direction of the force toward stronger magnetic intensity requires $\chi > 0$ and remains an explicit hypothesis of the model.

It is convenient to introduce the effective inertial energy density

$$\boxed{u_{\mathrm{eff}} \equiv \frac{W_i}{V_{\mathrm{eff}}}, \qquad \frac{\chi V_{\mathrm{eff}}}{W_i} = \frac{\chi}{u_{\mathrm{eff}}}.} \qquad (6.2)$$

Consequently, a trajectory measurement at fixed magnetic geometry constrains the ratio χ/u_{eff}, rather than either parameter independently. If the geometric factors

defining energy and interaction volume differ, u_{eff} includes their ratio; it should not be confused automatically with a locally measured electric or magnetic energy density.

6.2. Scaling of Magnetic Curvature

Let a field of characteristic amplitude B_m vary across a transverse length scale a. Its typical intensity gradient is of order B_m^2/a. Equation (6.1) then gives a characteristic curvature magnitude

$$\boxed{\kappa_{\mathrm{char}} \sim \frac{\chi\, g(\alpha)}{2\mu_0 u_{\mathrm{eff}}} \frac{B_m^2}{a}.} \qquad (6.3)$$

If the wave interacts with this gradient over a longitudinal distance ℓ, the associated small-angle deflection is of order

$$\boxed{|\theta_{\mathrm{out}}| \sim \frac{\chi\, g(\alpha) B_m^2}{2\mu_0 u_{\mathrm{eff}}} \frac{\ell}{a},} \qquad (6.4)$$

up to a dimensionless factor determined by the detailed field profile and impact parameter. This scaling emphasizes three effects: the deflection grows with the square of the external field amplitude, increases with the longitudinal interaction length, and decreases with the effective inertial energy density.

For saturated, geometrically similar tubular configurations, Parts B1–B2 motivate the approximate relations

$$W_i = C u_s R^2 L, \qquad V_{\mathrm{eff}} = C_V R^2 L. \qquad (6.5)$$

Thus

$$\boxed{u_{\mathrm{eff}} = \frac{C}{C_V} u_s, \qquad \frac{\chi V_{\mathrm{eff}}}{W_i} = \frac{\chi C_V}{C u_s}.} \qquad (6.6)$$

The explicit dependence on transverse radius R and coherent length L cancels *only* when the saturation energy density, relative geometry, and response coefficient remain unchanged. No universal independence from wavelength λ follows: u_s, C/C_V, or χ may depend on the actual field organization and wavelength.

6.3. Localized Gaussian Field: Analytical Deflection

For comparison with Section 5, use the illustrative intensity distribution

$$B_e^2(x,z) = B_m^2 \exp\left(-\frac{x^2}{a^2} - \frac{z^2}{\ell^2}\right). \qquad (6.7)$$

This expression specifies a scalar intensity profile, not a complete divergence-free vector field. Its use with $g(\alpha) \simeq 1$ assumes a suitable approximately axial local field orientation. A physical finite-length field must satisfy $\nabla \cdot \mathbf{B}_e = 0$ and may contain additional components.

Define the dimensionless interaction strength

$$\boxed{\eta \equiv \frac{\chi V_{\mathrm{eff}} B_m^2}{2\mu_0 W_i} = \frac{\chi B_m^2}{2\mu_0 u_{\mathrm{eff}}}.} \qquad (6.8)$$

For an incoming wave initially parallel to z with impact parameter b, the weak-deflection approximation replaces $x(z)$ by b on the right-hand side of the trajectory equation. Integration along the full interaction region gives

$$\boxed{\theta_{\mathrm{out}} \simeq -\frac{2\sqrt{\pi}\,\eta \ell b}{a^2} \exp\left(-\frac{b^2}{a^2}\right).} \qquad (6.9)$$

For $b > 0$ the negative sign denotes bending toward the magnetic-intensity axis. At fixed field parameters, the largest magnitude in this approximation occurs at $|b| = a/\sqrt{2}$. The approximation requires both a small net angle and a displacement

during transit that is small enough for $x \simeq b$ to be valid.

6.4. Representative Numerical Values

Take $B_m = 0.20\ \mathrm{T}$, $a = 1{,}000\ \mathrm{km}$, $\ell = 2{,}000\ \mathrm{km}$, and $b = 500\ \mathrm{km}$. These are illustrative input parameters, **not** a reconstructed field of a measured solar structure. Equation (6.9) then becomes

$$\boxed{|\theta_{\mathrm{out}}| \simeq \frac{9.0631 \times 10^{9}}{u_{\mathrm{eff}}}\,\chi \quad \mathrm{arcsec},} \tag{6.10}$$

where u_{eff} is expressed in $\mathrm{J\,m^{-3}}$ and the trial angular factor is set to unity. The numerical coefficient includes the conversion $1\ \mathrm{rad} = 206{,}264.806\ \mathrm{arcsec}$.

For the idealized reference choice $\chi = 1$, the conditional angular predictions are:

Effective energy density u_{eff} ($\mathrm{J\,m^{-3}}$)	Predicted $\lvert\theta_{\mathrm{out}}\rvert$ (arcsec)
5.0×10^{8}	18.13
1.0×10^{9}	9.06
1.6×10^{9}	5.66
2.0×10^{9}	4.53
5.0×10^{9}	1.81

Table 1. Conditional deflection angles for a selected Gaussian magnetic-intensity profile and the unverified choice $\chi = 1$.

Conversely, a target angle of 5 arcseconds for this *chosen* profile requires

$$\boxed{\frac{u_{\mathrm{eff}}}{\chi} \simeq 1.81 \times 10^{9}\ \mathrm{J\,m^{-3}}.} \tag{6.11}$$

Equation (6.11) does not establish the actual energy density of an electromagnetic wave: it is an inverse constraint obtained by selecting a desired deflection. Likewise, a numerical agreement after independently adjusting both χ and u_{eff} would not constitute an independent validation of the physical mechanism.

For comparison with Section 5, the illustrative choice $\eta = 10^{-5}$ gives $\theta_{\mathrm{out}} \simeq -5.69$ arcseconds. For $\chi = 1$ this corresponds to $u_{\mathrm{eff}} \simeq 1.59 \times 10^{9}\ \mathrm{J\,m^{-3}}$ under the same assumed profile.

6.5. Axis Approach and Required Magnetic Length

For an extended guiding field with $B_e^2(x) = B_m^2 \exp(-x^2/a^2)$, the near-axis restoring constant from Section 5 is

$$\boxed{k_g = \frac{\sqrt{2\eta}}{a}, \qquad z_{\mathrm{axis}} = \frac{\pi}{2k_g} = \frac{\pi a}{2\sqrt{2\eta}}.} \tag{6.12}$$

The first-axis-crossing distance z_{axis} applies to an undamped wave that enters parallel to the axis and remains within a sufficiently long, nearly uniform guide. With $a = 1{,}000\ \mathrm{km}$ and $\eta = 10^{-5}$, the result is

$$\boxed{k_g \simeq 4.47 \times 10^{-9}\ \mathrm{m^{-1}}, z_{\mathrm{axis}} \simeq 351{,}000\ \mathrm{km}.} \tag{6.13}$$

This is much longer than the $2{,}000\ \mathrm{km}$ longitudinal scale used in the localized example of Section 6.4. The two field configurations are therefore physically distinct: the localized region can impart an angular deflection, whereas approach to the axis requires continued guiding over a much longer path at the same interaction strength.

A useful *order-of-magnitude* focusing condition for an approximately constant near-axis guide of length L_g is $k_g L_g \gtrsim \pi/2$, or

$$\boxed{\eta \gtrsim \frac{\pi^2 a^2}{8L_g^2}.} \tag{6.14}$$

For $a = 1{,}000\ \mathrm{km}$ and $L_g = 2{,}000\ \mathrm{km}$, this idealized estimate would require $\eta \gtrsim 0.31$, vastly larger than 10^{-5}. The condition is not directly applicable to a Gaussian field that decays along z; it instead demonstrates why a substantial finite deflection should not be confused with magnetic capture.

6.6. Radiative Damping and Energy Cost

In a near-axis guide, Section 5 introduced the phenomenological equation

$$\boxed{x'' + \gamma x' + k_g^2 x = 0, \qquad \gamma = \frac{\zeta P_{\mathrm{rad}}}{cW_i}.} \quad (6.15)$$

The factor $\zeta > 0$ is a directional-momentum asymmetry parameter. It is not determined by the total radiated power alone. Define the radiative energy-loss length $L_E = cW_i/P_{\mathrm{rad}}$. Then

$$\boxed{\gamma = \frac{\zeta}{L_E}, \qquad \gamma_{\mathrm{crit}} = 2k_g.} \quad (6.16)$$

For the illustrative guide parameters of Equation (6.13), $\gamma_{\mathrm{crit}} \simeq 8.94 \times 10^{-9}\ \mathrm{m}^{-1}$. If $\zeta = 1$, the corresponding critical-loss length is $L_E \simeq 112{,}000\ \mathrm{km}$. Under a constant fractional-loss approximation, the remaining energy after a path of length z is $W_i(z)/W_i(0) = \exp(-z/L_E)$.

At the undamped first-crossing distance of approximately $351{,}000\ \mathrm{km}$, a constant critical damping value would imply only about 4.3% of the initial propagation energy remaining. This is an energy-cost illustration, not a self-consistent solution at such large losses: variations in the wave geometry, the interaction coefficient, and potentially k_g must then be considered. A more weakly damped trajectory may approach the axis through gentle oscillations with substantially smaller losses.

6.7. Radius Reduction and the Limits of Similarity

For the hypothetical saturated family with fixed C, u_s, and coherent length L, gradual attenuation obeys

$$\boxed{\frac{R(z)}{R_0} = \sqrt{\frac{W_i(z)}{W_i(0)}}.} \quad (6.17)$$

For example, retaining 90% of the original propagation energy implies $R/R_0 = \sqrt{0.90} \simeq 0.949$. The radius decreases by about 5.1%. This reduction alone does not damp the transverse propagation angle. Damping requires a preferential transverse momentum flux, as made explicit in Section 5.

If the effective interaction volume and propagation energy remain proportional to $R^2 L$ during attenuation, their ratio is unchanged and the magnetic curvature coefficient need not vary despite the reduced radius. This cancellation fails if the transverse profile, saturation density, coherent length, or response coefficient changes. The proposed geometrical scaling therefore supplies a useful conditional prediction, not a general conservation law.

6.8. Quantitative Status and Experimental Requirements

The numerical calculations above establish consistent scaling relations **conditional on** the effective magnetic-force hypothesis. The dominant dimensionless strength is $\eta = \chi B_m^2/(2\mu_0 u_{\mathrm{eff}})$, with the geometry and impact parameter determining how that strength translates into an observable angle. The damping regimes involve the additional ratio $\gamma/(2k_g)$, whose value depends on the directional distribution of any emitted radiation.

Several quantities remain to be determined independently: (i) the sign and magnitude of χ from a consistent electromagnetic momentum balance; (ii) the positive propagation energy density and effective interaction geometry; (iii) the actual angular dependence of the coupling; and (iv) the directional radiation response responsible for γ. The present model does not claim that a static magnetic field deflects freely propagating light under ordinary linear vacuum Maxwell electrodynamics. A nonzero result requires the additional proposed structured-wave interaction to be physically established.

A discriminating test should therefore measure angular deflection against a controlled transverse gradient, reverse the field polarity without changing its squared magnitude, vary the field amplitude and incidence angle, and separately assess any attenuation or loss of coherence. Section 7 develops these requirements into experimental tests and potential falsification criteria.

7. Experimental Tests and Predictions

7.1. Purpose of Experimental Verification

The effective framework developed in Sections 3–6 proposes that a coherent tubular electromagnetic wave may respond to a spatially nonuniform external magnetic field through a transverse interaction. Such a response has **not** been derived from conventional linear vacuum electrodynamics. Consequently, the proposed deflection must be regarded as an experimentally testable additional hypothesis rather than a recognized consequence of Maxwell's equations.

The principal task of an experiment is to distinguish a genuine change in the propagation direction of light from changes caused by material media, plasma, field-induced motion of optical components, and ordinary instrumental effects. A useful test should determine the field geometry independently and should measure not only the angular displacement but also the field-strength, gradient, orientation, and wavelength dependences. Where possible, a null result should be translated into a numerical bound on the proposed coupling.

The earlier analysis gives the approximate paraxial force law

$$\boxed{\frac{d^2x}{dz^2} = \frac{\chi}{2\mu_0 u_{\text{eff}}}\, g(\alpha)\, \frac{\partial B_e^2}{\partial x}, \quad u_{\text{eff}} \equiv \frac{W_i}{V_{\text{eff}}}.} \tag{7.1}$$

Here χ is an unknown response coefficient, u_{eff} the effective propagation-energy density, and $g(\alpha)$ a proposed angular response; the trial choice is $g(\alpha) = \cos^2\alpha$. The independent physical origin of these quantities remains open. Equation (7.1) supplies a quantitative target for tests without presupposing that the predicted force exists.

7.2. Uniform-Field and Gradient Controls

The first distinction is between a homogeneous magnetic field and a nonuniform one. The proposed gradient law predicts no transverse force when the magnetic intensity is spatially constant across the wave trajectory:

$$\boxed{\nabla_\perp B_e^2 = 0 \quad \Rightarrow \quad \mathbf{F}_\perp = 0.} \tag{7.2}$$

A measurement sequence should therefore compare three states: zero applied magnetic field, an approximately homogeneous applied field, and a field with a calibrated transverse intensity

gradient. These states should be matched as closely as possible in mechanical loading, heating, electrical drive, and other experimental conditions.

If the proposed mechanism is correct, an observed deflection should track the *transverse gradient of the squared field magnitude*, not simply whether a magnet is present. A nonzero signal in a homogeneous-field control, at an otherwise comparable operating condition, would indicate an unmodeled contribution or a failure of the simple gradient law.

The external field is a vector field subject to $\nabla \cdot \mathbf{B}_e = 0$. Real laboratory magnets have fringe fields and field-direction changes; hence a proposed profile of B_e^2 alone does not fully determine α or the predicted trajectory. Three-dimensional field mapping is required in the measurement volume.

7.3. Field-Amplitude and Polarity Tests

For fixed field shape and orientation, multiplying the applied magnetic field by a factor s changes B_e^2 and its gradient by s^2. In the weak-deflection regime, Equation (7.1) therefore predicts

$$\boxed{\theta(sB_e) \simeq s^2\theta(B_e).} \qquad (7.3)$$

More generally, if the magnetic-field amplitude is controlled independently of its spatial profile, the measured angle should follow a quadratic dependence on amplitude at sufficiently small deflections. This test probes a distinctive scaling relation rather than merely the existence of an angular shift.

The proposed force also depends on B_e^2, so complete reversal of the external field vector gives

$$\boxed{\theta(-\mathbf{B}_e) \simeq \theta(\mathbf{B}_e)} \qquad (7.4)$$

provided the geometry, wave response coefficient, and angular factor are unchanged under reversal. Field reversal thus provides a useful control: a signal odd in the magnetic-field polarity would not agree with the elementary squared-intensity law. However, an even-in-field artifact may imitate Equation (7.4); polarity symmetry alone is not decisive evidence.

A reversed *transverse intensity gradient*, in contrast, should reverse the sign of the transverse deflection. The distinction between reversing $\mathbf{B}_e$ and reversing $\nabla_\perp B_e^2$ should be made explicit in the experimental protocol.

7.4. Angular Dependence of the Interaction

The model proposes that the magnetic coupling decreases as the angle α between the propagation direction and the local external magnetic field increases. Its provisional angular function is

$$\boxed{g(\alpha) = \cos^2\alpha.} \qquad (7.5)$$

Under a controlled comparison in which the transverse gradient and other wave parameters are held fixed, the predicted relative response is

$$\boxed{\frac{\theta(\alpha)}{\theta(0)} \simeq \cos^2\alpha.} \qquad (7.6)$$

For example, this trial law predicts relative values of 1, 0.75, 0.25, and 0 at $0°$, $30°$, $60°$, and $90°$, respectively. These are predictions of the *assumed angular function*, not deductions from the internal E–B–P equations.

In practice, changing the field orientation may also change the gradient sampled by the ray. The projected gradient $\nabla_\perp B_e^2$ must therefore be evaluated for each

configuration. Without this correction, an apparent angular dependence could simply reflect a change in the force geometry.

If reproducible deflection is detected, angular scans can determine whether the response follows $\cos^2\alpha$, a different smooth function, or no systematic orientation dependence. A signal that persists at 90° under otherwise identical conditions would falsify the specific trial function in Equation (7.5), though not every conceivable structured-wave interaction.

7.5. Laboratory Differential-Deflection Experiment

A candidate test uses a stable, narrow optical beam traversing a magnetized region while its exit direction is measured relative to a reference path. The magnetic volume should be free of solid optical elements and, as far as practical, evacuated. Beam position and beam angle should be recorded separately; a lateral displacement at a single detector is not, by itself, sufficient to establish an angular deflection.

A possible differential protocol consists of: (i) mapping the full three-dimensional magnetic field, including fringe regions; (ii) recording the beam with the magnet inactive; (iii) recording with a calibrated uniform-field control; (iv) recording several gradient strengths and polarities; and (v) varying the incident beam position and angle. Repeated switching and reference-channel measurements help isolate drift from a field-correlated optical response.

For a weakly deflected ray entering at impact parameter b, integration of Equation (7.1) along an approximately straight reference path gives

$$\boxed{\Delta\theta_x \simeq \frac{\chi}{2\mu_0 u_{\mathrm{eff}}}\int_{z_1}^{z_2} g\left(\alpha(b,z)\right)\left.\frac{\partial B_e^2(x,z)}{\partial x}\right|_{x=b} dz.} \qquad (7.7)$$

This relation makes it possible to compute a *field integral* from the mapped magnet rather than using a nominal peak field as a proxy for the interaction. It also identifies the parameter combination to be constrained experimentally.

A strong result would require systematic exclusion or quantitative control of residual gas and plasma refraction, magnetic forces on optical mounts, magnetic or thermal changes in windows and detector electronics, air-path fluctuations, vibrations, and stray light. Conventional linear Maxwell theory predicts no magnetic deflection of light in an ideal source-free vacuum; established nonlinear quantum-vacuum effects under strong magnetic fields are a separate, much smaller and differently modeled class of phenomena. Any observed signal must be assessed against these alternatives.

7.6. Wavelength, Energy, and Transverse-Structure Tests

For a family of geometrically similar saturated wave structures, Section 6 predicts cancellation of the explicit radius and coherent-length factors in the ratio V_{eff}/W_i. In that restricted case, the curvature coefficient is

$$\boxed{\frac{\chi V_{\mathrm{eff}}}{W_i} = \frac{\chi C_V}{C u_s}.} \qquad (7.8)$$

A fixed magnetic geometry would then give the same deflection for different transverse radii R **if** the saturation density, geometry ratio, angular response, and χ are unchanged. The model does not yet establish these conditions across different

wavelengths, powers, or coherence lengths.

Measurements at several wavelengths could test whether a single response ratio accounts for all results, or whether the coupling depends on frequency or wave organization. Likewise, measurements with different beam powers and transverse profiles may help distinguish an intrinsic wave response from optical-system artifacts, although the incident beam diameter is not automatically identical to the microscopic transverse radius R postulated for an individual coherent structure.

An important experimental limitation is therefore that the model has not yet supplied a direct procedure to prepare or independently measure the hypothesized individual-wave radius R. No claim of a parameter-free wavelength-independent prediction is justified until that structural mapping is available.

7.7. Magnetic Guidance, Damping, and Radiation

Sections 5–6 describe a separate limiting configuration in which an external field provides an extended guiding region with an approximately symmetric magnetic-intensity maximum along an axis. Near that axis, the effective transverse equation can be written

$$\boxed{x'' + \gamma x' + k_g^2 x = 0.} \qquad (7.9)$$

The restoring coefficient k_g^2 is set by the assumed gradient interaction. The damping coefficient γ is phenomenological and is positive only if additional radiation or another momentum-exchange channel removes transverse momentum in the required direction. Its existence does not follow solely from energy attenuation.

The three regimes are: overdamped approach without repeated axis crossings ($\gamma > 2k_g$); critical approach ($\gamma = 2k_g$); and damped oscillation around the axis ($0 < \gamma < 2k_g$). They are possible solutions of Equation (7.9), **not** three individually established properties of light in a magnetic field.

An experimental search for guidance would require an extended magnetically structured path, measurements of beam position and direction at multiple longitudinal locations, and sufficient spatial resolution to distinguish approach to the axis from repeated crossings. A localized angular deflection alone is not evidence of long-range capture. In a finite guide, a ray may exit before reaching or settling onto the axis.

If damping is attributed to internal E–B–P rearrangement, the proposed radiation channel must satisfy both energy and momentum conservation. A necessary experimental program would compare angular damping with optical-power loss, spectral changes, off-axis scattered emission, and changes of coherence. A reduction in optical power without preferential transverse-momentum transport would not demonstrate the proposed mechanism.

7.8. Parameter Identification and Falsification Criteria

A single measured deflection constrains, at best, the combination χ/u_{eff} for a specified geometry. It cannot establish $\chi = 1$ or the microscopic energy density independently. If an experiment yields an angular uncertainty $\delta\theta$ consistent with zero, Equation (7.7) gives a bound

$$\boxed{\left|\frac{\chi}{u_{\mathrm{eff}}}\right| \lesssim \frac{2\mu_0\,\delta\theta}{\left|\int_{z_1}^{z_2} g\,(\alpha)\;\partial_x B_e^2\,dz\right|},} \qquad (7.10)$$

provided the field integral is nonzero and measurement uncertainties and systematic effects are correctly included. The precise confidence level should be stated by the experiment. Where the integral vanishes by symmetry, a null result cannot constrain the coupling through this relation.

The tests should examine the following discriminating requirements together: dependence on a nonzero transverse intensity gradient; approximately quadratic scaling with field amplitude at weak deflection; invariance under complete field-polarity reversal; reversal of deflection when the transverse gradient is reversed; and the measured angular dependence at a controlled gradient. Guidance and radiative damping would be additional tests rather than prerequisites for detecting an initial transverse impulse.

A reproducible, artifact-controlled result incompatible with these scaling and symmetry relations would reject the **specific effective law** used in Sections 4–6. Conversely, agreement with the relations would support its phenomenological usefulness but would not by itself establish the proposed tubular E–B–P microscopic mechanism. Independent determination of the propagation-energy density, the field configuration, and the directional radiation response would be needed to test the complete physical interpretation.

The principal experimental priority is therefore a differential measurement of deflection with a fully characterized magnetic gradient and a credible null control. Such a measurement can provide a direct constraint on the proposed interaction before the additional question of long-range magnetic guidance is addressed. [9], [10]

8. Discussion and Conclusions

8.1. Scope of the Proposed Magnetic-Deflection Mechanism

This study has developed an effective description of magnetic deflection for the tubular electromagnetic-wave structure introduced in Parts B1–B4. Its central proposal is that a spatially nonuniform external magnetic field modifies the internal balance of the coupled electric (E), magnetic (B), and displacement-current-related intermediate (P) configurations. A transverse interaction may then redirect the momentum of the complete propagating structure. The framework is not offered as a derivation of such an interaction from the conventional linear Maxwell equations in vacuum.

The analysis separates two issues that are sometimes conflated. The first is the *mechanical consequence* of a transverse force acting on electromagnetic momentum. The second is the *physical origin and magnitude* of the transverse force. The former can be treated through momentum balance; the latter remains the defining hypothesis to be established independently.

The effective inertia of a coherent wave segment is represented by its positive propagation energy W_i:

$$\boxed{m_i = \frac{W_i}{c^2}, \qquad \mathbf{p} = \frac{W_i}{c}\,\hat{\mathbf{t}}.} \tag{8.1}$$

Here m_i is an energy-equivalent inertial mass, not a rest mass. The approximately balanced positive and negative internal energy contributions are distinguished from the propagation energy; their magnitudes must not be counted again as independent energy contributions. The P configuration participates in internal reorganization, but its quantitative

contribution to propagation inertia has not been separately established.

8.2. Effective Force, Curvature, and Angular Response

The candidate transverse-force law is

$$\boxed{\mathbf{F}_\perp = \frac{\chi V_{\text{eff}}}{2\mu_0}\, g(\alpha)\, \nabla_\perp B_e^2, \qquad g(\alpha) = \cos^2\alpha.} \tag{8.2}$$

The projected gradient is taken perpendicular to the instantaneous direction of propagation. A positive χ describes the hypothesized force toward greater external magnetic intensity; $\chi = 1$ is an idealized reference choice, not a derived result. The angular function is likewise a proposed response law requiring independent verification. A real external magnetic configuration must be treated as a vector field satisfying $\nabla \cdot \mathbf{B}_e = 0$.

When the magnitude of momentum is approximately constant, the resulting trajectory curvature is

$$\boxed{\kappa = \frac{\chi V_{\text{eff}}}{2\mu_0 W_i}\, g(\alpha)\, |\nabla_\perp B_e^2|.} \tag{8.3}$$

This expression predicts no transverse deflection in a strictly homogeneous intensity profile, within the stated force law. It predicts an approximately quadratic dependence on externally applied magnetic-field amplitude when the field shape and orientation are held fixed. Reversing the entire magnetic-field vector does not reverse the predicted force, whereas reversing the transverse gradient does. These consequences provide ways to test the effective interaction without presupposing a particular microscopic explanation.

The magnetic-boundary picture developed in Section 3 offers a possible physical interpretation of internal field adaptation. However, a scalar magnetic-pressure step by itself does not imply the assumed attractive force: the full vector electromagnetic stress and field response are required. The sign and value of χ must therefore remain explicit rather than being inferred from the negative internal binding-energy convention alone.

8.3. Trajectories and the Conditions for Magnetic Guidance

In an externally prescribed field with a symmetric magnetic-intensity maximum along a guiding axis, the proposed force acts as a local restoring interaction for small transverse displacement. Under a paraxial and locally constant-coefficient approximation, the equation of motion is

$$\boxed{\frac{d^2x}{dz^2} + \gamma\frac{dx}{dz} + k_g^2 x = 0.} \tag{8.4}$$

The restoring coefficient $k_g^2 > 0$ is determined by the assumed magnetic coupling and local field profile. The coefficient γ describes an *additional* effective loss of transverse motion. In this approximation three regimes are possible: an overdamped, comparatively slow approach to the axis ($\gamma > 2k_g$); a critically damped approach ($\gamma = 2k_g$); and damped crossings of the axis ($0 < \gamma < 2k_g$).

All three are valid mathematical solutions of the effective guiding equation. Their physical realization depends on the force law, the field geometry, the initial direction, and the magnitude and sign of the damping response. No unique trajectory has been established by the present analysis. In particular, attraction toward a magnetic-intensity maximum does not automatically imply capture: without damping, the wave can cross the axis and continue oscillating, or leave a

finite magnetic region with a net angular deflection.

The longitudinal extent of the field is consequently crucial. A weak transverse force may produce measurable bending over a localized region without guiding the wave to the axis. Extended guidance requires a sufficiently long region of restoring interaction and, for asymptotic settling, an effective mechanism that decreases transverse motion.

8.4. Internal Reorganization, Radiation, and Damping

The E–B–P picture allows internal field distributions to change while the wave is being deflected. Such reorganization may involve an additional outward electromagnetic energy flux. Nevertheless, a change in the direction of internal momentum, or a reduction in total energy, does not by itself establish radiation damping of the trajectory.

For an additional radiated power P_{rad}, define the transverse momentum carried away per unit time by

$$Q_x = \frac{1}{c}\int n_x \frac{dP_{\mathrm{rad}}}{d\Omega}\, d\Omega. \qquad (8.5)$$

If the outgoing radiation carries only the transverse momentum associated with emission along the current ray direction, the radiation terms cancel in the equation for its angle. Angular damping requires a directional excess of outgoing transverse momentum. A provisional description is

$$\boxed{\gamma = \zeta \frac{P_{\mathrm{rad}}}{cW_i}, \qquad \zeta > 0,} \qquad (8.6)$$

where ζ parametrizes the required angular asymmetry of the emitted momentum. Neither the existence of such an asymmetry nor the sign or magnitude of ζ has yet been calculated from the internal E–B–P fields. This is a distinct open problem, rather than a consequence of radiative energy loss alone.

Under the saturated-geometry assumption and at constant coherent length, gradual reduction of propagation energy would also give

$$\boxed{\frac{R}{R_0} \simeq \sqrt{\frac{W_i}{W_{i0}}}.} \qquad (8.7)$$

This radius change describes structural attenuation; it does not independently determine angular damping. The two responses need to be measured or derived separately.

8.5. Quantitative Interpretation and Parameter Dependence

The estimates in Section 6 demonstrate how the assumed interaction translates into a numerical angular deflection for a specified magnetic-intensity profile. They are conditional examples, not confirmed predictions for a particular solar or laboratory field. A Gaussian field profile is useful for analytic evaluation but must be replaced by a physically consistent three-dimensional magnetic field in any detailed comparison with observation.

For saturated and geometrically similar wave structures, the relations $W_i = Cu_s R^2 L$ and $V_{\mathrm{eff}} = C_V R^2 L$ imply

$$\boxed{\frac{\chi V_{\mathrm{eff}}}{W_i} = \frac{\chi C_V}{C u_s}.} \qquad (8.8)$$

Thus the explicit factors $R^2 L$ cancel in the curvature law if u_s, the geometrical ratios, and χ remain unchanged. This is a conditional scaling result, not a proof that deflection is independent of wavelength, coherence, or wave structure. The characteristic saturated energy density u_s

has not yet been independently determined from the model.

A single angular-deflection measurement primarily constrains the ratio χ/u_{eff}, where $u_{\mathrm{eff}} = W_i/V_{\mathrm{eff}}$. Consequently, choosing $\chi = 1$ does not by itself produce a parameter-free prediction. Separate information about the propagation-energy density or the magnetic-response coefficient is required to determine the other quantity.

8.6. Experimental Discrimination and Open Questions

The most direct test is a differential beam-deflection measurement in a well-characterized transverse magnetic-intensity gradient, with a comparable homogeneous-field control. The experiment should independently establish the beam angle and lateral displacement and determine the full vector magnetic field, including fringe regions. Systematic effects associated with residual media, optical mounts, windows, magnetic forces on equipment, temperature, and vibrations must be distinguished from a genuine change of propagation direction.

The proposed model can be challenged through a combination of gradient reversals, magnetic-amplitude scaling, full field-polarity reversal, and angular orientation scans. A null result can place a bound on χ/u_{eff} for a specified field integral. Agreement with the scaling relations would support the *effective law*, but would not, by itself, demonstrate the hypothesized microscopic tubular structure. Conversely, a reproducible violation of its defining gradient, amplitude, or angular relations would reject the corresponding version of the proposed force law.

The principal unresolved questions are the derivation of the transverse force from a self-consistent E–B–P field configuration; the sign and value of χ; the form of $g(\alpha)$; an independent determination of the effective energy density and transverse geometry; and the calculation of the outward radiative momentum flux required for $\gamma > 0$. A complete analysis must conserve energy and momentum for the electromagnetic wave, external-field sources, and any additional radiation together. [6], [9], [10], [11]

8.7. Conclusions

The present study has formulated an effective connection between electromagnetic-wave inertia, a hypothesized magnetic-gradient force, and the resulting change in trajectory. It shows that, **if** the proposed transverse interaction exists, the curvature is governed by the ratio of magnetic force to propagation energy. Under additional assumptions about an extended guiding field and a directional damping mechanism, the same framework admits gradual alignment, critical nonoscillatory alignment, and weakly damped oscillation around a magnetic-intensity axis.

The analysis does not establish that static external magnetic fields deflect light in source-free vacuum, nor does it derive the force coefficient or radiative damping from Maxwell's equations. Instead, it specifies the additional physical hypotheses required, their mathematical consequences, and the measurements capable of constraining or falsifying them.

The principal contribution of Part D3 is therefore a compact, testable mathematical framework for investigating the proposed magnetic interaction of structured electromagnetic waves.

References

[1] Rozman, F. *Part B1 – Physical Structure of the Electromagnetic Wave.* Unified Electromagnetic Theory of Matter and Light, Section B, manuscript, 2026.

[2] Rozman, F. *Part B2 – Stability, Coupling, and Dimensions.* Unified Electromagnetic Theory of Matter and Light, Section B, manuscript, 2026.

[3] Rozman, F. *Part B3 – Electromagnetic Interaction in the Photoelectric Effect.* Unified Electromagnetic Theory of Matter and Light, Section B, manuscript, 2026.

[4] Rozman, F. *Part B4 – Unified Electromagnetic Theory of Matter and Light.* Section B, manuscript, 2026.

[5] Poynting, J. H. *On the Transfer of Energy in the Electromagnetic Field.* Philosophical Transactions of the Royal Society of London 175 (1884), 343–361. https://doi.org/10.1098/rstl.1884.0016

[6] Jackson, J. D. *Classical Electrodynamics, 3rd ed.* John Wiley & Sons, 1998.

[7] Landau, L. D., and Lifshitz, E. M. *The Classical Theory of Fields, 4th ed.* Course of Theoretical Physics, Vol. 2, Pergamon Press, 1975.

[8] Born, M., and Wolf, E. *Principles of Optics: Electromagnetic Theory of Propagation, Interference and Diffraction of Light, 7th expanded ed.* Cambridge University Press, 1999.

[9] Heisenberg, W., and Euler, H. *Folgerungen aus der Diracschen Theorie des Positrons.* Zeitschrift für Physik 98 (1936), 714–732. https://doi.org/10.1007/BF01343663

[10] Bialynicka-Birula, Z., and Bialynicki-Birula, I. *Nonlinear Effects in Quantum Electrodynamics: Photon Propagation and Photon Splitting in an External Field.* Physical Review D 2 (1970), 2341–2345. https://doi.org/10.1103/PhysRevD.2.2341

[11] Ejlli, A., Della Valle, F., Gastaldi, U., Messineo, G., Pengo, R., Ruoso, G., and Zavattini, G. *The PVLAS Experiment: A 25 Year Effort to Measure Vacuum Magnetic Birefringence.* Physics Reports 871 (2020), 1–74. https://doi.org/10.1016/j.physrep.2020.06.001